SENSING IN-SITU TEMPERATURES BY COORDINATES IN FUSED FILAMENT FABRICATION FOR IDENTIFYING INTERLAYER ANISOTROPIC MECHANICAL PROPERTIES AND ENABLING POST-FEM ANALYSIS

Amlie, Erik;
Fylling, Emil;
Eikevåg, Sindre Wold;
Nesheim, Ole S.;
Steinert, Martin;
Elverum, Christer W.

NTNU

ABSTRACT

In Additive Manufacturing (AM), new generations of polymer composites presented as engineering-grade materials provide high-end mechanical properties with the design freedom AM provides. Interlayer anisotropy is the main challenge in both in-situ optimization and post-analysis in transitioning from prototypes to high-performance components in fused filament fabrication (FFF). Recent studies show a direct correlation between layer fusion temperature and mechanical properties. In this paper, we present synchronized position and temperature data and study how a component changes based on layer height and geometry. An IR sensor transfers data while printing a G-code generated by FullControllGcode, printing in a single direction and recording temperature in front of the nozzle. Results show that within each layer, a Δt of 20°C at thinner geometries, the heat loss will provide a reduction in mechanical properties and further heat loss occurs when moving away from the heated bed. By using the presented temperature mesh in further studies, post- printed anisotropic components can be analyzed by FEM, and the FFF process can be adaptively optimized based on location, size and geometry.

Keywords: Additive Manufacturing, Open source design, 3D printing, Thermal analysis, Layer temperature

Contact:
Nesheim, Ole S.
NTNU
Norway
ole.s.nesheim@ntnu.no

1 INTRODUCTION

In recent times additive manufacturing (AM) has become extremely popular in boosting innovation and product development while keeping waste and costs low. Material extrusion, also called Fused Filament Fabrication (FFF), are one of the most popular AM methods for polymers and is represented in the professional and hobby (Open-source) markets with hundreds of machine-makers and filament producers (Saleh Alghamdi et al., 2021). The next-generation polymer composites with engineering-grade material properties when injection molded are currently being adapted for use in FFF, and due to the design freedom caused by the layer-by-layer build-up, designers will be able to use FFF in industrial applications like aerospace, medical implants, and sports equipment (Das et al., 2020). High-performance engineering thermoplastics (HPET), e.g., polyether ether ketone (PEEK) are chemically stable, heat-resistant, and form-stable in extreme conditions. In return FFF manufacturing of HPET's require significant innovations in printer hardware to accommodate increased nozzle and chamber temperatures (Weyhrich and Long, 2022).

Components made by FFF have anisotropic mechanical properties depending on path orientation and raster angle (Ziemian et al., 2012). In addition, FFF components tend to have high porosity due to gaps, pores, and poor weld properties between layers due to inadequate bed leveling leading to delamination (Koch et al., 2017) or too low chamber temperature (Zawaski and Williams, 2020).

The delamination effects are accelerated by thermal contraction and expansion, especially for large area prints where the layer time is long enough for the material to cool and contract (warp) before the next layer is deposited. Fibre-reinforced filaments can halt this effect by decreasing the thermal expansion coefficient but works best when chamber-temperature is right below the glass transition temperature for the extruded material (Billah et al., 2019).

Even dogbones printed flat on a heated bed experience significant cooling during short durations between layers, especially when fabricated in batches, increasing fragility due to longer convection cooling times with the surrounding atmosphere (Mantecón et al., 2022). Increasing the initial extrusion temperature enhances the mechanical properties of printed parts (Wach et al., 2018). Therefore, many material producers recommend annealing the parts after printing to reduce residual stress and increase interlayer diffusion. If provided with experimental mechanical properties, calculating thermal evolution between layers and predicting bonding strength is possible with transient heat equations and finite element analysis modeling (FEA) of a single line component (Khanafer et al., 2022). FEA computations for more complex geometries can optimize a part for stronger layer adhesion by altering the design of specific component sections to retain more heat between layers in a thermal layer design process (Bjørken et al., 2022).

Thermal evolution inside complex geometries is hard to predict. An experimental, in-process way of thermal mapping instead of complex heat equations for the FEA mesh used for bonding calculations would make it possible to document the calculated layer adhesion for individual components. Calculating bonding strength is possible because a printed part's UTS results from layer temperature (Bjørken et al., 2022) and parameters like chamber temperature (Zawaski and Williams, 2020). With enough experimental data, FEA could predict the bonding strength based on layer area, layer time, bed temperature, and chamber temperature for any printer or component, which could then be experimentally validated by continuous monitoring of the layer temperature during printing.

The open-source community within 3D printing software and hardware improvements have successfully made budget systems for printing HTEP's (Birkelid et al., 2022). Professional companies are achieving the same, but open-source electronics are contributing to scientific and technological innovation by connecting inventors and makers on a global scale (Oellermann et al., 2022). As a result, this article investigates the development of an open-source low-cost continuous layer-temperature mapping systems for any 3D printer by using commercially available temperature readers, open-source software libraries, and simple prototyping tools like laser cutting and 3D printing.

2   METHOD

An experiment is conducted to measure in situ interlayer temperature and coordinate measurements while printing a component in carbon fibre-reinforced nylon, PA-CF30. The component with a selection of geometries is needed to validate that the method can measure differences in layer temperature and identify the Δt within each layer. The following sections describe hardware setup, experiment and machine programming, and data acquisition with analysis to achieve thermal mapping of fused filament fabricated components. FFF components are inherently anisotropic due to different mechanical properties parallel or normal to the layer orientation and raster angle (Koch et al., 2017). Therefore, the experiment uses hardware and custom GCode to map previous layer temperature to identify interlayer bonding and mechanical anisotropy based on results by Bjørken et al. (2022).
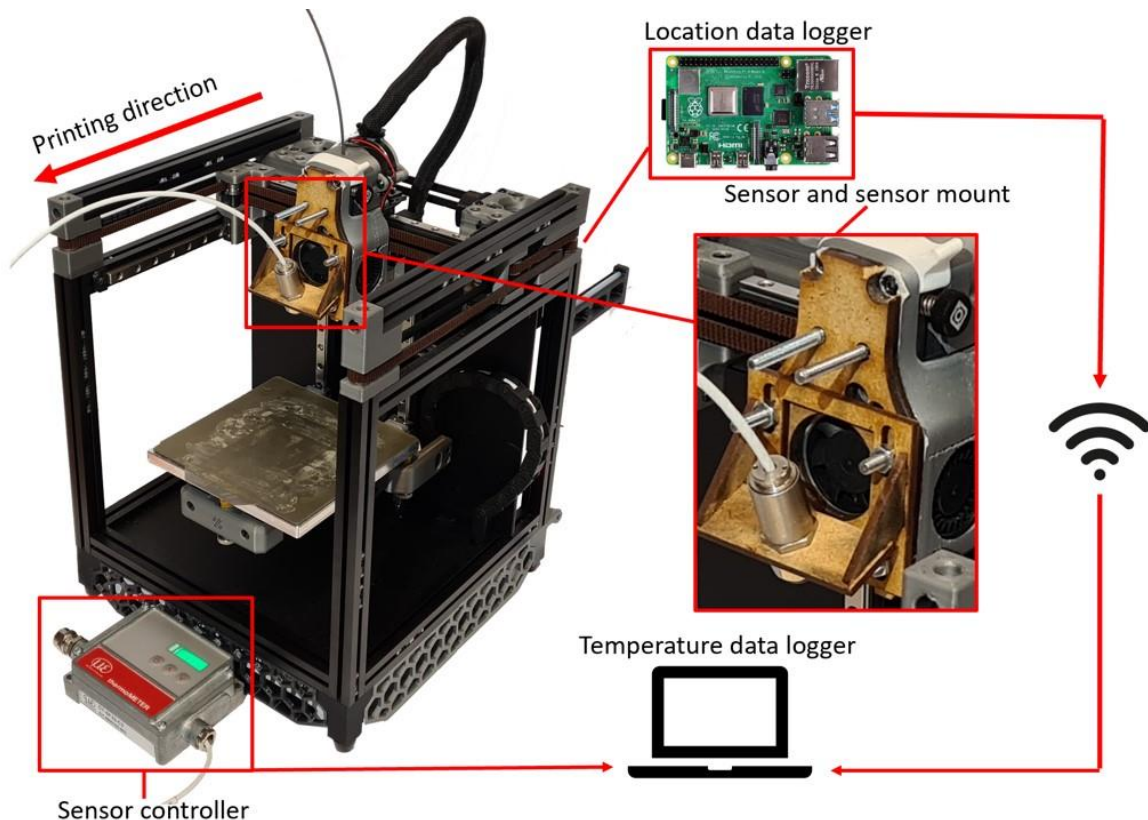
2.1   Hardware and setup

Figure 1. Hardware setup and communication paths

Figure 1 shows the hardware setup and how location and temperature data are synchronized. A Voron V0.1 upgraded with a high-flow dragon hot end (LDOMotors Co, 2022) was chosen for possible open-source modification capabilities and performance compared to other FFF printers. Voron printers are known for their build quality, customizability, precision at high speeds, and ability to print engineering materials at high flow. Controlling the printer over IOT/WiFi was done with a Raspberry Pi 3B+ with Octopi installed. Octopi UI was used because of its great open-source forums and libraries of custom plugins that yield further customizability. A CT-SF22 infrared temperature sensor (Micro-Epsilon, 2022) with an additional close proximity lens, ensuring a focal point of 0.6mm diameter 10mm from the lens, was added to the extruder assembly to measure the layer temperature. The recommended emissivity value for plastic in the IR-sensors manual used for this experiment was 0.95 (Micro-Epsilon, 2022). The IR-sensors data was logged using CompactConnect PC software found on the manufacturer's website. CompactConnect (Micro-Epsilon, 2022) software was run on a separate computer to log the infrared sensor through the sensor controller. The same computer ran a program to get the printer to log its location under printing. The laptop was connected to the Raspberry Pi on the printer through application programming interface (API) over Wifi. The filament used by the printer was a commercial-grade PolyMide PA6-CF from Polymaker (Polymaker, 2022). This filament was

continously dried in a PrintDry Filament Dryer PRO at 75°C before and during printing. For mounting the IR sensor, brackets were designed in Fusion 360 and laser cut from 3mm MDF sheets. The designed bracket has a fixed angle and is adjustable in height. The adjustability was necessary to calibrate the IR sensor to the smallest focal point. For accurately calibrating the IR sensor at the correct height, a simple laser-cut MDF jig that used the nozzle tip as height reference and heat block edges for axis parallelity was created. Aiming was done by seating the heat block and nozzle into a slot in the jig, before sliding the IR sensor into a notch on the jig and fastening the four screws to lock the position. The aiming should be sufficient for measuring in one direction at a set distance from the nozzle, as seen in Figure 2, but a custom G-code had to be made to obtain continuous readings with this simple IR sensor setup.
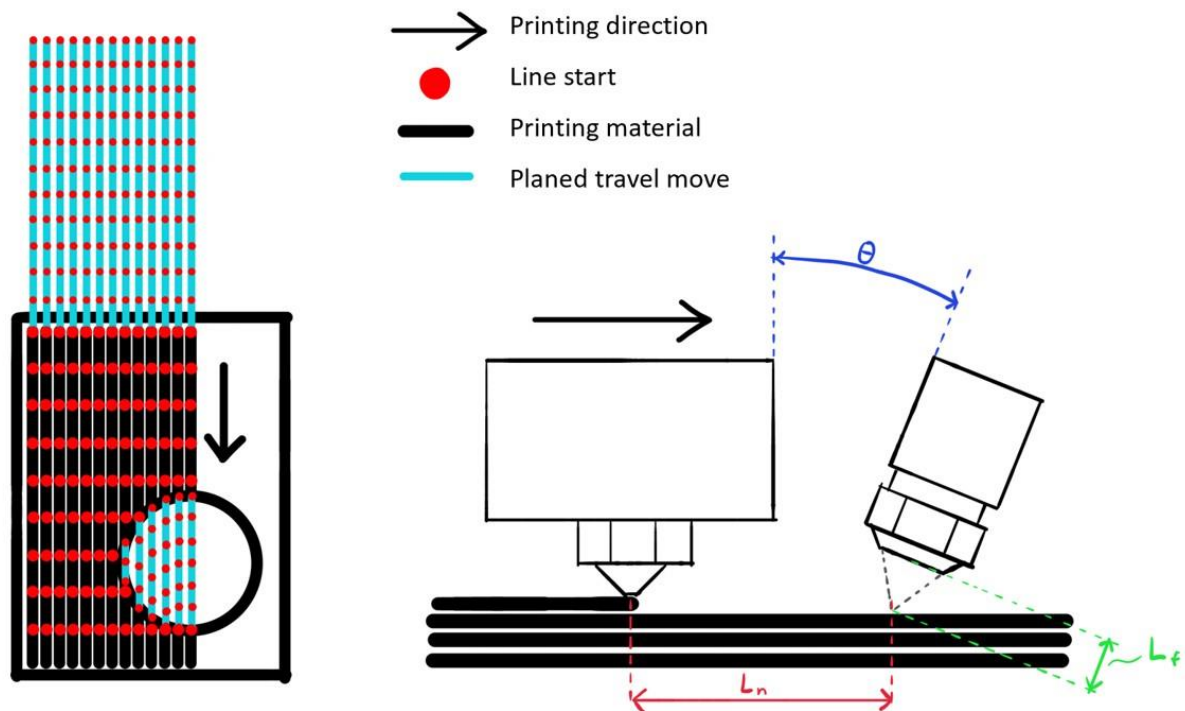
2.2 Experiment and G-code generation

Figure 2. G-code path illustrations and sensor orientation

The infrared sensor was mounted to the extruder with an offset angle and distance from the extruder (Figure 2). For the final setup, the L_n = 33mm and Θ = 22.5°. The distance and angle were restricted by the shape of the extruder while still getting the sensor close enough for a proof of concept. The sensor distance from the nozzle records temperature measurements 33mm in front of the nozzle while printing in the negative y direction in the coordinate system of the printer. The fixed sensor placement results in being unable to measure most of the print with common printing strategies and available slicers. Creating a custom G-code was necessary to get a complete measurement of each layer. In Figure 2, one can see a top-down view of a single layer during the printing process. The infrared sensor mounted to the extruder can only measure in front of the nozzle while moving in the sensor direction. To enable the experiment to measure as much of the layer as possible, the infill was designed only to print in the negative y direction. FullControl GCODE Designer (Gleadall, 2021) was used to create a custom infill. Once the infill G-code worked as intended, it was discovered that the method for logging the extruder's position could only register at the end of commands. Therefore, infill lines were only registered at the ends of the infill, not providing a temperature mesh. A temperature mesh was created by dividing infill lines into 0.6mm sections along the initial infill line, as seen in Figure 2, by the red point marking starting points for each 0.6mm line. The printer would continue to print like normal with no stops, but it was now possible to get position logging inside the part. As seen in Figure 2 , the sensor has an L_n = 33mm offset in front of the nozzle introducing a new problem of the sensor measuring outside the part in the negative y direction and now being able to

measure far enough in the positive y direction. Using FullControll, additional travel to move 33mm in the positive y direction was added, and the area where the sensor is outside the part was filtered out later in the software. This travel move can be seen in Figure 2 as the turqouise line above the part. This line was also divided into 0.6mm lines to create points for logging position during the measurement of the part.
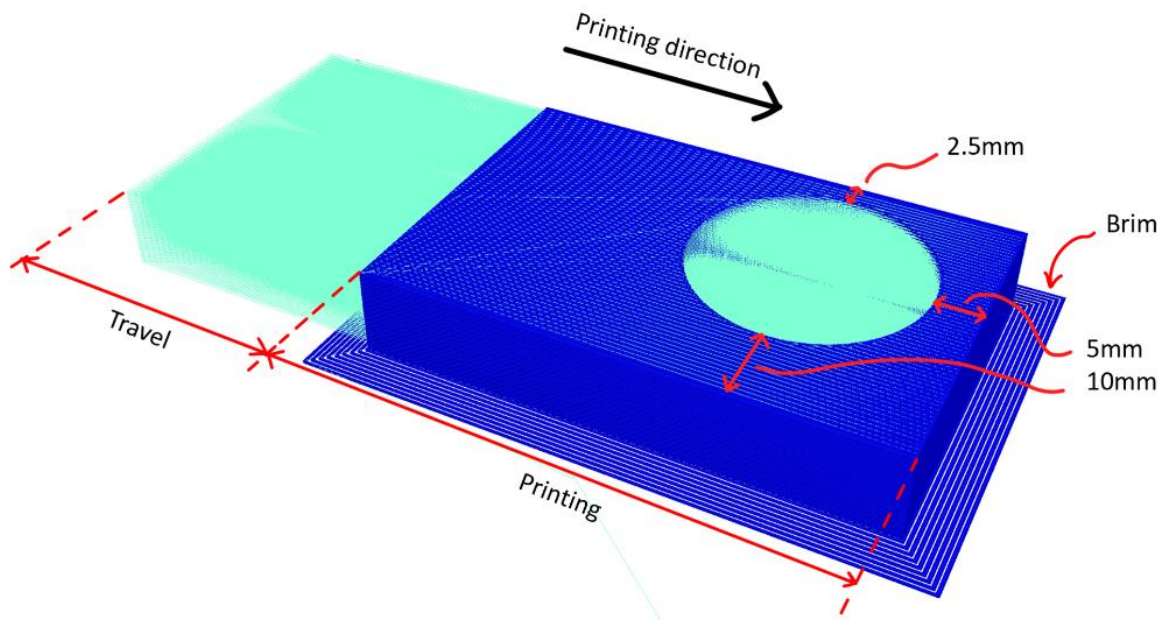

Figure 3. G-code preview and wall-thickness dimensions

Figure 3 shows the entire G-code-generated part in 3d representation. A brim was added to the first layer of the print to ensure that the print would adhere properly to the build plate during printing. The G-code ended up being large in size due to the dividing of infill into small lines making this part over 370 000 lines of G-code. Due to the designed shape of the object, there is a travel move during the printing of the infill. The travel move was divided into small lines to generate the desired amount of logging points for the coordinates. The test object was designed to contain different features that will experience different layer temperatures. On one side of the object is a large area with full infill. This area is thought to maintain heat for longer. On the other side of the object, a 27.5mm diameter hole was added, with the center at x=63.75 and y=28.75. The hole was placed offset to create three different wall thicknesses for analyzing temperature differences. The three walls created with this hole were 10mm, 5mm, and 2.5mm, as seen in Figure 3.

2.3 Data acquisition and analysis

For the first iteration of logging the temperature synchronized with XYZ positions, a custom Python plugin for the printer's control software, Octopi, was hypothesized. However, neither the Klipper software installed on the motor controlling unit (MCU) nor the UI software, Octopi, installed on the Raspberry Pi have standard hooks to pull out the current position through the API.

To create the temperature mesh, the standard temperature logging software CompactConnect, supplied with the IR sensor, logged the temperature with timestamps at a 10Hz sample rate in tabulator-separated ".dat" files.   In the terminal of the Octopi UI, it is possible to send G-codes during printing. Sending "M114" yields a response string with current global XYZ and E coordinates, time, and date. At 10Hz, "M114" was sent to the terminal over IoT through the API in the Octopi software. Octopi was set to automatically log all information sent and received in the terminal in a "serial.log" file that is downloadable through the UI settings. After a print job, the IR-sensor temperature log and the Octopi terminal log, "serial.log", were saved for analysis.

Python reads the respective logs as pandas data frames, filter and extract the interesting columns: Time and date from both logs, X, Y, and Z, from "serial.log" and "TProc" from the CompactConnect ".dat" logs. Then a Python program converts the data frames into comma-separated values (CSV) file format. Finally, another python program takes in the respective CSV files and merges them on time and date within a tolerance of 0.01s with the pandas.merge_asof function and applies the matplotlib.pyplot library to create temperature graphs, 3D scatterplots, and 2D scatterplots of XYZ-positions with color mapping according to the IR sensor.

3   RESULTS

This section presents a 3D thermal plot retrieved from the experiment comparing the physical component with a 3D representation of the component with thermal information in Figure 4. Then three layers are presented with a 2D thermal plot and a graph showing the thermal measurement over different geometries in the layers in Figure 5.
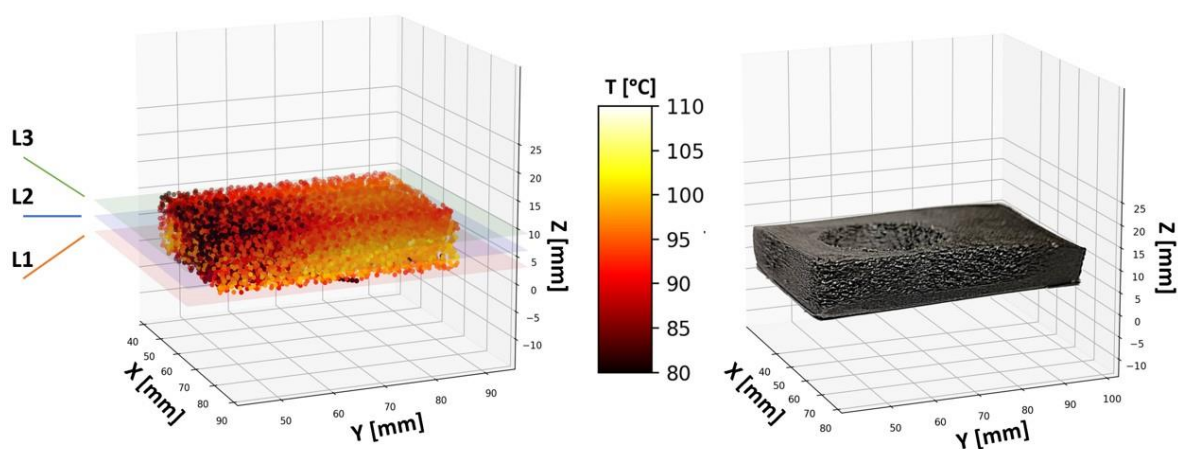

Figure 4. The physical component and a 3D thermal scatterplot representation of the component

The plot in Figure 4 clearly shows a thermal trend in different sections of the component. The measurements inside the model's hole should be discarded. The big trends are that the temperature seems to be higher in layers closer to the bed, and it is evident that the component layer temperature on the side without a hole has the highest temperature. Dividing the part into quadrants with the origin in the centre, the first quadrant achieved the highest last-layer temperature of around 100°C, while the third quadrant containing the thinnest section around the hole was between 85°C and 90°C in the top layers.

In Figure 4, L1, L2, and L3 are represented with translucent planes. The planes are at Z=3.2mm, 6.5mm, and 9.5mm, respectively. Figure 5 shows thermal scatterplots of the component at L1, L2, and L3 and raw IR sensor data when traversing the different interesting component sections during printing.
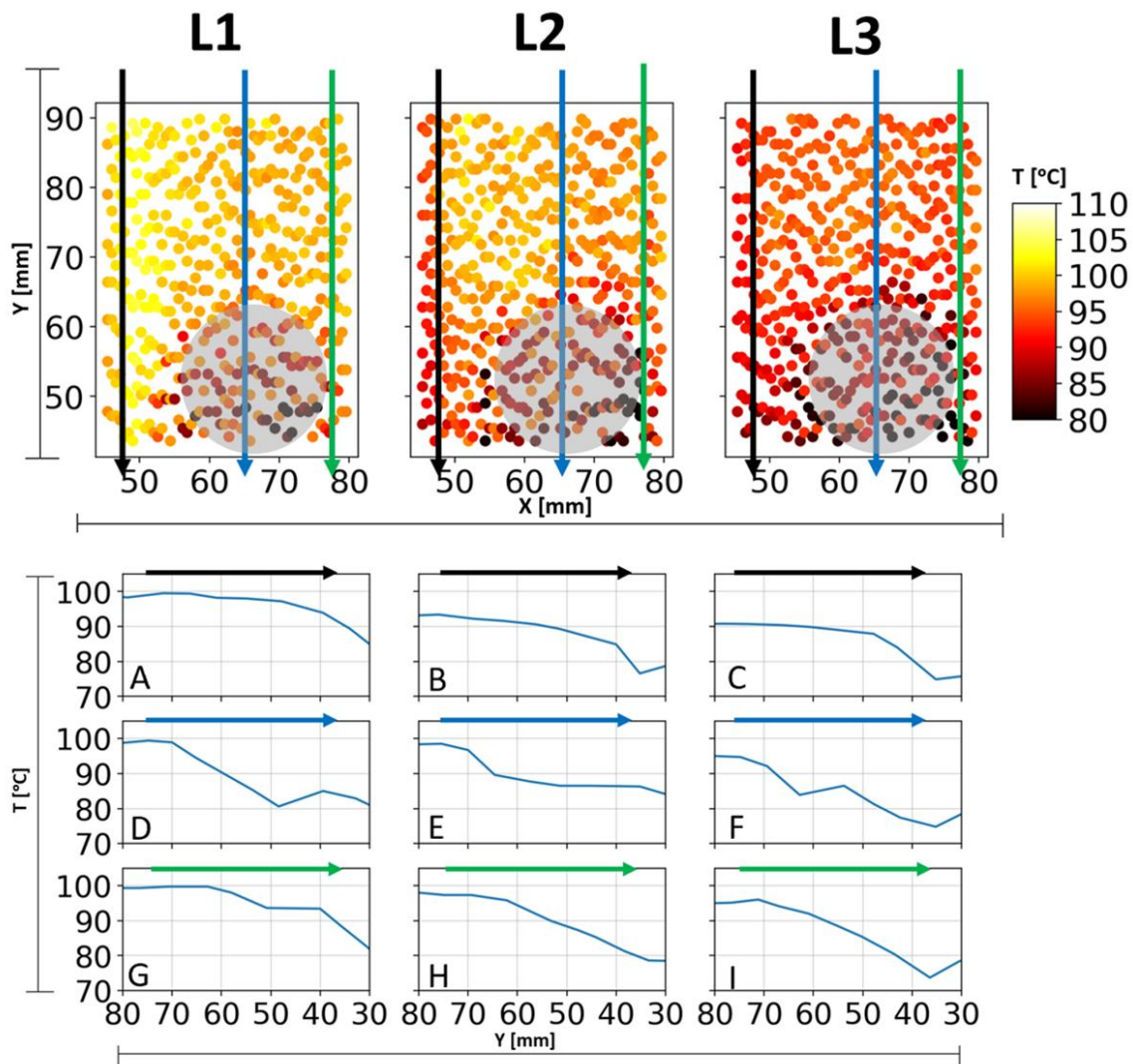
Figure 5. 2D thermal graphs in the layers L1, L2 and L3

Both L1, L2, and L3 in Figure 5 support the trends observed in Figure 4. The part has a higher previous layer temperature in quadrants one and four than the parts of the block without a hole. The graphs drawn from the IR sensor readings at specific X-values also support this trend by showing that the temperature decreases the closer the IR sensor gets to the hole, represented by shaded circles in Figure 5. With the graphs plotted out like in A-I in Figure 5, it becomes evident that the general temperature in the layers decreases with the print's height, and the change is more significant in the earlier layers. The effects of the hole geometry become visible with the temperature becoming lower closer to the hole. Along with the effects of the distance to the hole, there is an apparent effect of the wall thicknesses. The results show that thinner walls seem to give a greater temperature drop through the paths in graphs A-I; for example, G and I have a higher temperature drop from Y=60 to Y=40 than A and C, respectively. Path G drops 7°C, A drops 5°C, while I drops 13°C, and C decreases 10°C. A similar trend is observed between the 2.5mm wall and 5mm wall, plot G is around 92°C at 5mm wall thickness, and graph D is 85°C at 2.5mm wall thickness.

4 DISCUSSION

The method chosen for achieving data logging during printing introduced some limitations. With the script pushing G-code command "M114" at 10Hz, only getting the location info at the end of move commands during printing creates a sampling rate lower than 10Hz and unpredictable patterns. In addition, the temperature log was completely separate and measured at 10Hz, causing the separate logs not to match their timestamps and may have caused a significant loss of data where the location and temperature data points do not line up and are left out of the plot.

To achieve such location logging by pushing the "M114" command to the printer and having sufficient location points during the infill printing, it was necessary to have the G-code consisting of many small lines per line of infill. The constant pushing of the "M114" command, combined with the small rapid lines, may have caused an overload of commands to the printer, causing it to take random pauses during printing and travel moves to process the following commands. These pauses were un-periodic and at seemingly random locations. These pauses can affect the cooling time of the measured layer and cause inconsistencies in the total measurement.

To further improve the measurement process of this experiment, an external method for measuring the location of the extruder should be used. A TOF(time of flight) sensor on each axis or a mechanical method like a linear potentiometer would be a possible solution. Using external sensors, one can log the location and temperature in the same log with identical timestamps. Having one log file would remove the issue of data loss due to timestamps not aligning and remove the need for large G-code files.

The test prints used in this paper do not accurately represent the real-world application of 3d-printing technology, caused by the un-traditional infill pattern used and the unnecessary travel moves added for the temperature measurements. With the temperature sensor only being able to measure in the negative y direction, having an infill pattern exclusively printing in the negative y direction was necessary to get measurements across the entire layer. Using this printing method for traditional 3d-printed parts can cause the part to be offset as it is printed higher due to the extruder nozzle only making proper contact with the printed part in one direction and can therefore exert some forces along that move. Having multiple sensors on different sides of the extruder would make it possible to extract measurements during more traditional printing. Also, by using machine learning to extract the correct temperature measurements from an otherwise noisy dataset, the sensor can be used with traditional slicer-generated G-code. However, a limited amount of points can still provide point-based material properties of high-performance polymers.

In Figure 4, one can see how the heat of the heated bed affects the print at the early layers and how the effect wears out the higher the print goes. This effect can also be seen in Figure 5, where the temperature of plots a, b, and c can be compared to analyze the effect of height. If one would compare a, b, and c at 70mm, one can see that from a to b, there is a more significant temperature decrease, of around 8°C, than from b to c, which is only changed by around 2°C. This difference would suggest that the effect is wearing off with height. The phenomenon of the bed causing a higher layer temperature for the first layers is supported by Vaes et al. (2019), who found that the stable temperature shifted downwards as the part became taller.

This experiment used an infrared sensor to measure the layer temperature. The infrared sensor was chosen above a thermal camera due to its accuracy and ease of integration into the system. Having a thermal camera may give a better image of the thermals of the entire visible part of the print, but getting the thermal camera to read a specific point ahead of the nozzle at all times may not be possible. Using a thermal camera in a heated chamber is also challenging, and with the need for a heated chamber for optimal temperatures under the printing of high-performance polymers, it would not be beneficial to create a proof of concept with this method. In this study, the interest lies in finding the temperature in specific points before the next layer of filament is deposited. The infrared sensor was optimal for this task, but it can be challenging, mainly because of the accuracy needed when mounting the sensor to the extruder. The distance from the printed part and the alignment to the printed direction are essential. The distance needs to be correct due to the focal point of the sensor. Too far or too close would cause the sensor to measure more than the one desired line of infill. The alignment of the sensor to the printing direction is crucial due to too far right or left would result in measuring one line of infill too far ahead or measuring the line that was just printed. Inaccurate calibration of the sensor position would result in invalid data. An alignment jig was used to solve this, and the sensor was aligned

according to the heater block, but this solution is suspected of not being entirely accurate. A test may need to be developed to verify the alignment of the sensor.

In Figure 4, there seems to be much noise in the measurements in the hole because the focal point of the IR sensor increases in size when the relative distance from the IR-sensor lens to the component increases (Micro-Epsilon, 2022). This part of the temperature plot should not be considered usable data as it does not measure the current layer, if the part at all. The hole is being measured and plotted like the rest of the part due to the method needed to get the measurement does not differentiate from travel within the part and printed area. A possible solution to remove such sources of error could be to filter out unrealistic spikes/drops in value that happens when the sensor is measuring outside the part.

4.1 Application and significance of findings

The layer temperature monitoring system presented in this study is valuable for several applications. For decades, the research community has proposed that AM will overtake traditional material removal production methods with AM of high-temperature engineering thermoplastics. As a result, a vast amount of research papers focus on improving hardware, materials, and software for AM, especially FFF systems. The machines are more precise, the speed is higher and the material flow is reaching new limits, but yet the flawed anisotropic mechanical properties of components fall short of injected molded or machined parts. This experiment was conducted at room temperature with an unrealistic G-code, but it proves the ability to measure even minor temperature deviance due to geometry differences, and the measuring system will be able to see small implications of different parameter changes with a thermal map. A complete thermal map of the component yields full process control of how bed temperature, nozzle temperature, print speed, chamber temperature, humidity, and layer area impacts the actual layer bonding. By measuring the temperature in situ, the Δt within each layer can be used to determine the mechanical properties, as demonstrated by Bjørken et al. (2022). The Δt within each layer will also wary depending on size and geometry, and change as layers change during the component print. Finally, temperature measurements directly correlate to mechanical properties, and after the print is completed, the component can be accurately simulated in anisotropic finite element analysis (Khanafer et al., 2022).

5 CONCLUSION

In this paper, sensing of layer temperature is added to FFF and synchronized to a custom-generated G-code. The G-code is generated in FullControlGcode with a single printing direction, offset to component for temperature sensing and a coordinate mesh. A component is produced with in situ mesh showing changes in layer fusion temperatures according to layer height and geometry. As layer fusion temperature correlates to mechanical properties, in situ temperature measurements allow for identifying in-layer Δt at different printing parameters for the best fit to mechanical properties. The presented temperature mesh allows for post-print finite element analysis of anisotropic components produced by fused filament fabrication.

REFERENCES

Billah, K.M.M., Lorenzana, F.A.R., Martinez, N.L., Chacon, S., Wicker, R.B., Espalin, D., 2019. Thermal Analysis of Thermoplastic Materials Filled with Chopped Fiber for Large Area 3D Printing. University of Texas at Austin. https://doi.org/10.26153/tsw/17325

Birkelid, A.H., Eikevåg, S.W., Elverum, C.W., Steinert, M., 2022. High-performance polymer 3D printing– Open-source liquid cooled scalable printer design. HardwareX 11.

Bjørken, O.U., Andresen, B., Eikevåg, S.W., Steinert, M., Elverum, C.W., 2022. Thermal Layer Design in Fused Filament Fabrication. Applied Sciences 12, 7056. https://doi.org/10.3390/app12147056

Das, A., Chatham, C.A., Fallon, J.J., Zawaski, C.E., Gilmer, E.L., Williams, C.B., Bortner, M.J., 2020. Current understanding and challenges in high temperature additive manufacturing of engineering thermoplastic polymers. Additive Manufacturing 34, 101218. https://doi.org/10.1016/j.addma.2020.101218

Gleadall, A., 2021. FullControl GCode Designer: Open-source software for unconstrained design in additive manufacturing. Additive Manufacturing 46, 102109. https://doi.org/10.1016/j.addma.2021.102109

Khanafer, K., Al-Masri, A., Deiab, I., Vafai, K., 2022. Thermal analysis of fused deposition modeling process based finite element method: Simulation and parametric study. Numerical Heat Transfer, Part A: Applications 81, 94–118. https://doi.org/10.1080/10407782.2022.2038972

Koch, C., Van Hulle, L., Rudolph, N., 2017. Investigation of mechanical anisotropy of the fused filament fabrication process via customized tool path generation. Additive Manufacturing 16, 138–145.

LDOMotors Co, L., 2022. Voron 0.1 Kit [WWW Document]. LDO Docs. URL https://docs.ldomotors.com/en/voron/voron01 (accessed 11.23.22).

Mantecón, R., Rufo-Martín, C., Castellanos, R., Diaz-Alvarez, J., 2022. Experimental assessment of thermal gradients and layout effects on the mechanical performance of components manufactured by fused deposition modeling. Rapid Prototyping Journal 28, 1598–1608. https://doi.org/10.1108/RPJ-12-2021-0329

Micro-Epsilon (Ed.), 2022. Operating instructions Thermometer CT.

Oellermann, M., Jolles, J.W., Ortiz, D., Seabra, R., Wenzel, T., Wilson, H., Tanner, R., 2022. Harnessing the Benefits of Open Electronics in Science. Integrative and Comparative Biology 62, 1061–1075. https://doi.org/10.1093/icb/icac043

Polymaker, 2022. PolyMide_PA6_CF_TDS_V5.pdf.

Saleh Alghamdi, S., John, S., Roy Choudhury, N., Dutta, N.K., 2021. Additive Manufacturing of Polymer Materials: Progress, Promise and Challenges. Polymers 13, 753. https://doi.org/10.3390/polym13050753

Vaes, D., Coppens, M., Goderis, B., Zoetelief, W., Van Puyvelde, P., 2019. Assessment of Crystallinity Development during Fused Filament Fabrication through Fast Scanning Chip Calorimetry. Applied Sciences 9, 2676. https://doi.org/10.3390/app9132676

Wach, R.A., Wolszczak, P., Adamus-Wlodarczyk, A., 2018. Enhancement of Mechanical Properties of FDM-PLA Parts via Thermal Annealing. Macromolecular Materials and Engineering 303, 1800169. https://doi.org/10.1002/mame.201800169

Weyhrich, C.W., Long, T.E., 2022. Additive manufacturing of high-performance engineering polymers: present and future. Polymer International 71, 532–536. https://doi.org/10.1002/pi.6343

Zawaski, C., Williams, C., 2020. Design of a low-cost, high-temperature inverted build environment to enable desktop-scale additive manufacturing of performance polymers. Additive Manufacturing 33, 101111. https://doi.org/10.1016/j.addma.2020.101111

Ziemian, C., Sharma, M., Ziemian, S., Ziemian, C., Sharma, M., Ziemian, S., 2012. Anisotropic Mechanical Properties of ABS Parts Fabricated by Fused Deposition Modelling, Mechanical Engineering. IntechOpen. https://doi.org/10.5772/34233